Characteristic Timescales of the Local Moment Dynamics in Hund's Metals

C. Watzenböck,[1] M. Edelmann,[2] D. Springer,[1] G. Sangiovanni,[2] and A. Toschi[1]
[1]Institute of Solid State Physics, TU Wien, 1040 Vienna, Austria
[2]Institut für Theoretische Physik und Astrophysik and Würzburg-Dresden Cluster of Excellence ct.qmat, Universität Würzburg, 97074 Würzburg, Germany

(Received 27 January 2020; accepted 16 July 2020; published 20 August 2020)

We study the characteristic timescales of the fluctuating local moments in Hund's metal systems for different degrees of correlation. By analyzing the dynamical spin susceptibility in the real-time domain, we determine the timescales controlling oscillation and damping of on-site fluctuations—a crucial factor for the detection of local moments with different experimental probes. We apply this procedure to different families of iron pnictides or chalcogenides, explaining the material trend in the discrepancies reported between experimental and theoretical estimates of their magnetic moments.

DOI: 10.1103/PhysRevLett.125.086402

Introduction.—Our perception of the natural world is significantly shaped by the properties of the detection process considered. One crucial aspect is the timescale of the probing mechanism: If this is larger than the typical timescale of the phenomenon under investigation, only averaged information will be gained.

Here, we focus on the detection of the local magnetic moments in correlated metallic systems. Their proper description is, indeed, a key to understanding many-electron systems beyond the conventional band-theory framework, being central to: Kondo physics [1,2], Mott-Hubbard [3–5] or Hund-Mott [6–10] metal-insulator transitions, quantum criticality of heavy fermion systems [11,12], magnetic and spectroscopic properties of Ni and Fe [13–15], and of unconventional superconductors [16,17].

Reflecting the high physical interest, several experimental procedures are used to detect the local magnetic moments and their manifestations [18]: measurements of static susceptibilities [13,18], inelastic neutron spectroscopy (INS) [19], by integrating over the Brillouin zone (BZ) [20], x-ray absorption or emission spectroscopy (XAS or XES), etc.

Whether it is possible to obtain an accurate description of the local moments largely depends on the relation between the intrinsic timescales of the experimental probes and those characterizing the dynamical screening mechanisms at work. The emerging picture is typically clear-cut if the screening processes are strongly suppressed: In Mott or Hund's-Mott insulating phases, a coherent description of the magnetic moment properties can be easily obtained in all experimental setups. A more complex, multifaceted situation characterizes systems where well preformed magnetic moments present a rich dynamics. Good examples are the strongly correlated metallic regimes adjacent to a Mott metal-insulator transition, or even better, compounds displaying a Hund's metal behavior [6,21], such as iron pnictides and chalcogenides [17].

In this Letter, we illustrate how to quantitatively estimate the characteristic timescales of fluctuating moments in many-electron systems within the regime of linear response. As a pertinent example, we apply this procedure to investigate the puzzling discrepancies between experimental and theoretical estimates of the magnetic moment size in the different families of iron pnictides or chalcogenides, clarifying the peculiar material dependence of this long-standing issue.

An intuitive picture.—For a transparent interpretation of our realistic calculations, we start from some heuristic considerations on the dynamics of the local magnetic moment $\vec{\mu} = g(\mu_B/\hbar)\vec{S}$ in a correlated metal. The relevant information is encoded in the time dependence of its correlation function

$$\mathcal{F}(t) \equiv \frac{1}{2} g^2 \frac{\mu_B^2}{\hbar^2} \langle \{\hat{S}_z(t), \hat{S}_z(0)\} \rangle, \tag{1}$$

where $g \cong 2$ is the Landé factor, μ_B the Bohr magneton and $\hat{S}_z = \sum_\ell \hat{s}_z^\ell$ the z component of the total spin moment hosted by the correlated atom (e.g., a transition metal element), built up by the unpaired electronic spins s_z of its partially filled d or f shells [18]. We stress that Eq. (1) describes both the static (thermal) and dynamic (Kubo) part of the response [22], which is needed for our study. In general, one expects the maximum values of $\mathcal{F}(t)$ at $t = 0$: This describes the instantaneous spin configuration of the system, often quite large in a multiorbital open shell due to the Hund's rule. Because of electronic fluctuations, the probability of finding a magnetic moment of the same size and the same orientation will be decreasing with time. At a first approximation, one can identify two distinct patterns for this process: (i) a gradual rotation (with constant amplitude) and (ii) a progressive reduction of the size of

the local moment. Within this simple picture, two characteristic time (and energy) scales for the local moment dynamics are naturally defined: (i) the period of the rotation ($t_{\bar{\omega}} \propto 1/\bar{\omega}$) and (ii) the characteristic time ($t_\gamma \propto \hbar/\gamma$) for the amplitude damping.

The values of the characteristic timescales may vary considerably from one material to another, with overall larger values associated to a suppressed electronic mobility. In the extreme case of a Mott insulator, one expects to observe long-living magnetic moments, consistent with the analytic divergence of the timescales found in the fully localized (atomic) limit ($t_{\bar{\omega}}, t_\gamma \to \infty$). On the opposite side, in a conventional (weakly correlated) metal, both scales will be extremely short, roughly of the order of the inverse of the bandwidth W of the conducting electrons ($t_{\bar{\omega}} \sim t_\gamma \propto \hbar/W$). The most interesting situation is realized in a correlated metallic context. Here, the slowing down of the electronic motion, induced by the electronic scattering, increases the values of both timescales that remain finite, nonetheless. The enhancement will depend on specific aspects of the many-electron problem considered, possibly affecting the two timescales in a different fashion: This leads to the distinct regimes of underdamped ($t_\gamma \gg t_{\bar{\omega}}$) and overdamped ($t_\gamma \ll t_{\bar{\omega}}$) local moment fluctuations, schematically depicted in Fig. 1. The actual hierarchy of the timescales will strongly impact the outcome of spectroscopic experiments. Further, quantitative information about the dynamics of the magnetic fluctuations at equilibrium may also provide important information for the applicability of the adiabatic spin dynamics [23–25] and, on a broader perspective, crucial insights for the highly nontrivial interpretation of the out-of-equilibrium spectroscopies.

Quantification of timescales.—The procedure to quantitatively estimate the characteristic timescales from many-electron calculations and/or experimental measurements relies on the Kubo-Nakano formalism for linear response. Here, we recall that the dynamical susceptibility is defined as

$$\chi(\tau) \equiv \langle T_\tau \hat{S}_z(\tau)\hat{S}_z(0)\rangle, \tag{2}$$

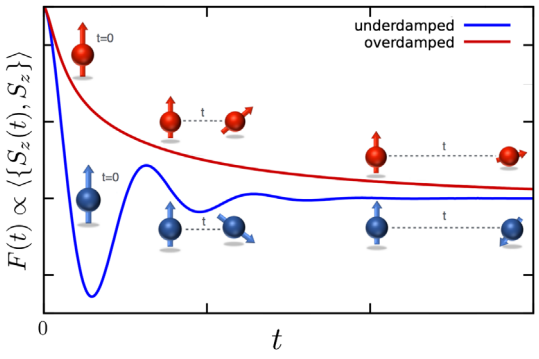

FIG. 1. Schematic representation of the time decay of local spin correlations in the underdamped or overdamped regimes.

in imaginary time (T_τ is the imaginary time-ordering operator). The corresponding (retarded) spectral functions $\chi^R(\omega)$ are obtained via analytic continuation of Eq. (2). The absorption component of the spectra, $\mathrm{Im}\chi^R(\omega)$, directly measurable (e.g., in INS), provides a direct route for quantifying the timescales. In particular, simple analytic expressions, directly derived for damped harmonic oscillators, can be exploited for fitting the (one or more) predominant absorption peak(s) of $\mathrm{Im}\chi^R(\omega)$. In the illustrative case discussed above, one has

$$\mathrm{Im}\chi^R(\omega) = A\frac{2\gamma\omega}{(\omega^2-\omega_0^2)^2+4\omega^2\gamma^2}, \tag{3}$$

where γ and ω_0 are the scales associated to the major absorption processes active in the system under consideration (with $\hbar = 1$), and the constant A reflects the size of the instantaneous magnetic moment. The expression is clearly generalizable to other cases, where more absorption peaks are visible in the spectra, as a sum of the corresponding contributions [26].

The full time-dependence of the fluctuating local moment, which will reflect the interplay of the timescales defined above, is eventually obtained via the fluctuation-dissipation theorem

$$\mathcal{F}(t) = \frac{1}{\pi}\int_0^\infty d\omega\, \cos(\omega t)\coth(\beta/2\omega)\mathrm{Im}\chi^R(\omega), \tag{4}$$

where $\beta = (k_B T)^{-1}$ is the inverse temperature.

The case of the Hund's metals.—While the procedure illustrated above is applicable to all spectroscopic experiments of condensed matter systems, we will demonstrate its advantages for studying Hund's metals [6,21], where the dynamics of fluctuating moments is of particular interest [47]. These systems can be viewed as a new "crossover"-state of matter, triggered by sizable values of the local Hubbard repulsion (U) and Hund's rule coupling (J), when the corresponding atomic shell is (about) one electron away from a half-filled multiorbital configuration. At strong coupling, the interplay between U and J can induce either a Mott or a charge-disproportionate Hund's insulator [9,48]. Out of half-filling, the competition between these two tendencies can also stabilize a metallic ground state in the presence of high values of the electronic interaction [6,9,48,49]. The emerging physics of a large local magnetic moment fluctuating in a strongly correlated metallic surrounding evidently represents one of the best playgrounds for applying our time-resolved procedure.

The prototypical class of materials displaying Hund's metal physics is represented by the iron pnictides or chalcogenides. These compounds, which often display unconventional superconducting phases upon doping, are also characterized by interesting magnetic properties [17,20,50]. Both the ordered magnetic moments (measured by neutron diffraction in the magnetically ordered phase) and the fluctuating moments (measured by INS in the

paramagnetic high-T phase) are reported to be systematically lower [51] in experiment than in (static) local spin density approximation calculations (predicting a large ordered moment of about $2\mu_B$ for almost all compounds of this class). It was also noted that, surprisingly, the larger discrepancies are found for the "less correlated" families 1111 (e.g., LaFeAsO) and 122 (e.g., $BaAs_2O_2$), which display milder quasiparticle renormalization effects and are characterized by lower values of the screened Coulomb interaction estimated in constrained random phase approximation [52]. Significantly smaller (or almost no) deviations are reported, instead, for the most correlated families such as the 11 subclass (e.g., FeTe), where relatively large local moments are found both in neutron experiments and theory. Previous dynamical mean-field theory (DMFT) studies of the INS results suggested [53–56] that the local spin fluctuations on the Fe atom—whose time-resolved description is the central topic here—may be responsible for the observed discrepancies. These works were restricted to one compound or (at most) one family only, and did not analyze the real-time domain. Hence, no definitive conclusion could be drawn about this issue, motivating the present computational material study.

Ab initio + DMFT calculations.—We report here on our density functional theory (DFT) + DMFT calculations [57,58] of the local spin susceptibilities in the iron pnictides or chalcogenides. Different from preceding works, we computed the spin-spin response functions on equal footing for several different compounds, chosen as representative of the most relevant families (1111, 122, 111, 11). As a step forward in the theoretical description, we put emphasis on a quantitative time-resolved analysis of the results, eventually allowing for a precise interpretation of the physics at play and of the spectroscopic results.

For our DMFT calculations [26,59], we considered a projection on the Fe-3d (maximally localized) Wannier-orbital manifold. We assume an on-site electrostatic interaction with a generalized (orbital-dependent) Kanamori form. The corresponding Hamiltonian reads

$$H = \sum_{\mathbf{k}\sigma lm} H_{lm}(\mathbf{k}) c^{\dagger}_{\mathbf{k}l\sigma} c_{\mathbf{k}m\sigma} + H_{\rm int}, \tag{5}$$

where l, m are orbital indices, $\mathbf{k}$ denotes the fermionic momentum, and σ, σ' the spin, and

$$\begin{aligned} H_{\rm int} = & \sum_{\mathbf{r}l} U_{ll} n_{\mathbf{r}l\uparrow} n_{\mathbf{r}l\downarrow} \\ & + \sum_{\mathbf{r}\sigma\sigma', l<m} (U_{lm} - J_{lm}\delta_{\sigma\sigma'}) n_{\mathbf{r}l\sigma} n_{\mathbf{r}m\sigma'} \\ & - \sum_{\mathbf{r}, l\neq m} J_{lm} [c^{\dagger}_{\mathbf{r}l\uparrow} c^{\dagger}_{\mathbf{r}l\downarrow} c_{\mathbf{r}m\uparrow} c_{\mathbf{r}m\downarrow} + c^{\dagger}_{\mathbf{r}l\uparrow} c^{\dagger}_{\mathbf{r}m\downarrow} c_{\mathbf{r}m\uparrow} c_{\mathbf{r}l\downarrow}], \end{aligned} \tag{6}$$

where $\mathbf{r}$ indicates the lattice site, and the realistic values of the screened electrostatic interactions U_{lm} and J_{lm} for the different materials have been taken from Ref. [52], as detailed in [26]. The orbitally averaged values of $\bar{U}, \bar{J}$ range from (2.53,0.38) eV for LaFeAsO to (3.41,0.48) eV for FeTe [26].

Our DMFT results are summarized in Fig. 2, where we show the dynamical spin susceptibility on the Fe atoms of all compounds considered in its different representations: imaginary time in the first-row panels [cf. Eq. (2)] which is the direct output [60] of the quantum Monte Carlo (QMC) solver, real frequency in the second row [from analytic continuations], real time in the third row [Eq. (1), via Eq. (4)]. In all cases, we performed our analysis not only for the full DMFT calculation (third column panels), which comprises—per construction—all purely local effects [63,64] of the DMFT self-energy and vertex corrections, but we also evaluate, separately, the corresponding "bubble" terms (i.e., $\chi_0 = -\beta GG$) either computed with the noninteracting Green's function ($G = G_0$, first column) or with the DMFT one ($G = G_{\rm DMFT}$, i.e., by including the DMFT self-energy, second column).

A quick glance at $\chi(\tau)$ already illustrates an important finding of our work: The different band structure of the materials as well as their self-energies does not generate by itself any distinguishable effects in the local moment dynamics (first two columns in Fig. 2). Instead, the definite material dependence observed is almost totally originated by vertex corrections (third column).

One can understand the overall material trend as follows: Instantaneous ($\tau = 0$) magnetic moments of similar (and large) sizes but subjected to quite different screening effects ($\tau \to (\beta/2)$). However, only the corresponding analysis of $\mathrm{Im}\chi^R(\omega)$ and $\mathcal{F}(t)$ allows us to extract clear-cut physical information. By looking at the data for $\mathcal{F}(t)$, we easily note that the moment dynamics described by the bubble terms (with or without $\Sigma_{\rm DMFT}$) is controlled by very short timescales for oscillation and damping (~0.5 fs), roughly corresponding to $\sim\hbar/W$. The inclusion of vertex corrections causes, instead, a significant and strongly material-dependent slowing down of the dynamics: In the "least-correlated" LaFeAsO, we already observe oscillation and damping over few fs (1 order of magnitude larger than in the noninteracting case). These timescales visibly increase considering more correlated families, up to the extreme case of FeTe, dominated by an extremely long decay over more than 25 fs.

The scenario emerging from the visual inspection of $\mathcal{F}(t)$ is supported, at a quantitative level, by the fit of the main absorption peaks of $\mathrm{Im}\chi^R(\omega)$, see Table I for details. The values t_γ and $t_{\tilde{\omega}}$ range from 3 to 30 fs, with an overall trend which trails the progressive reduction of the quasiparticle life time (t_{1P}) across the different families.

Spectroscopic measurements—The significant spread of the estimated timescale values directly affect the detectability of the local magnetic moments ($m_{\rm loc}$) in the iron pnictides or chalcogenides. While fast probes (e.g., XAS,

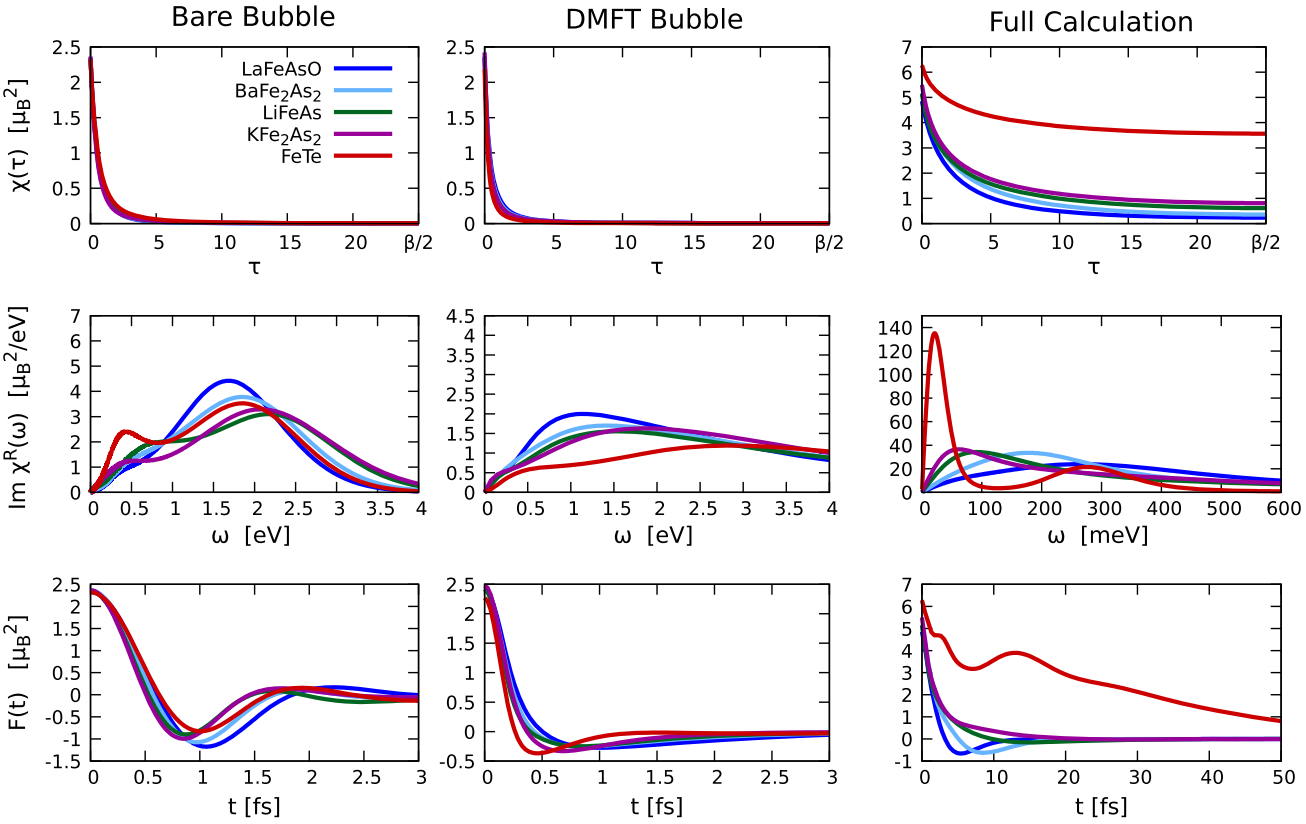

FIG. 2. Spin susceptibility of the $3d$-Fe atoms as a function of imaginary time (first row), corresponding absorption spectra in real frequency (second row) and correlation function in real time (third row), computed for different families of iron pnictides or chalcogenides at $\beta = 50$ eV^{-1} ($T \approx 232$ K) in the DFT + DMFT (third column), compared with the corresponding results of the bare (first column) and the DMFT (second column) bubble calculations.

XES) are able to detect the high-spin instantaneous configuration of these Hund's metals, the characteristic timescale of the INS ($t_{\mathrm{INS}} \simeq 5$–$10$ fs $\simeq \hbar/E_{\mathrm{INS}}$, with $E_{\mathrm{INS}} = \hbar\Omega_{\mathrm{INS}} \simeq 100$ meV [65]) are of the same order as those in Table I: time-averaging effects will, thus, lead to underestimation of the local magnetic moment

TABLE I. Fitting parameters ω_0 and γ of the absorption peak(s) computed in DMFT with Eq. (3) (first and second column, where the largest energy scale is marked in bold); effective lifetime $\chi(t \to \infty) \propto \mathrm{e}^{-t/t_\gamma}$ (third column); effective oscillation period $t_{\tilde{\omega}} = \hbar/\sqrt{\omega_0^2 - \gamma^2}$ (fourth column) and $t_{1P} = \langle \hbar/2Z_i \mathrm{Im}\Sigma_i(\omega \to 0)\rangle_{\text{all orb}}$ (fifth column) is the effective orbital averaged one-particle lifetime for the different material considered. See [26] for further details.

	ω_0 [eV]	γ [eV]	t_γ [fs]	$t_{\tilde{\omega}}$ [fs]	t_{1P} [fs]
LaFeAsO	**0.39**	0.35	1.9	3.8	30.80
$BaFe_2As_2$	**0.28**	**0.28**	2.4	15.2	19.96
LiFeAs	0.30	**0.58**	7.9	⋯	12.23
KFe_2As_2	0.51	**2.08**	10.3	⋯	9.08
FeTe	**0.029**	0.022	29.3	34.8	2.14

$$m^2_{\mathrm{loc}} = \frac{3}{\pi}\lim_{\Omega\to\infty}\frac{\int_{-\Omega}^{\Omega}\int_{\mathrm{BZ}}\mathrm{Im}\chi^R(\vec{q},\omega)b(\omega)\mathrm{d}\vec{q}\mathrm{d}\omega}{\int_{\mathrm{BZ}}\mathrm{d}\vec{q}} = \frac{3}{\pi}\lim_{\Omega\to\infty}\int_{-\Omega}^{\Omega}\mathrm{Im}\chi^R_{\mathrm{loc}}(\omega)b(\omega)\mathrm{d}\omega, \quad (7)$$

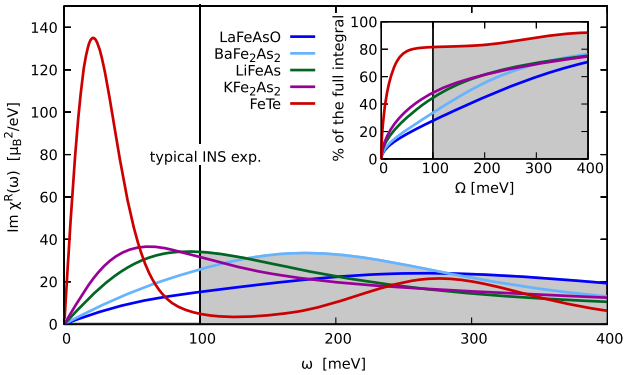

FIG. 3. Material dependence of the spin-absorption spectra in the different families of the iron pnictides or computed in DFT + DMFT, compared with the typical energy threshold (∼100 meV) of INS experiments. Inset: Corresponding fraction of m^2_{loc} obtained integrating Eq. (7) up to Ω.

where $b(\omega) = 1/(e^{\beta\omega} - 1)$ is the Bose-Einstein distribution function (with $\hbar = 1$). This is especially relevant for the less correlated compounds (LaFeAsO and $BaFe_2As_2$), where t_γ, $t_{\bar{\omega}} < t_{\mathrm{INS}}$. In families with higher degrees of freedom (e.g., for FeTe, where t_γ, $t_{\bar{\omega}} > t_{\mathrm{INS}}$), the averaging effect gets "mitigated," allowing the detection of larger magnetic moment sizes, consistent with fast probe XAS and XES experiments [67,68]. The material dependence of local moment dynamics is directly mirrored in the progressive red shift of the first-absorption peak in $\mathrm{Im}\chi^R(\omega)$, as shown in Fig. 3. Here, one can appreciate how an increasing part of the spin absorption spectra gradually enters the accessible energy window of the INS (main panel). This explains the progressively reduced discrepancies in the size of the magnetic moment (see inset) observed in the more correlated families of the iron pnictides or chalcogenides.

Conclusions.—We illustrated how to quantitatively investigate, on the real-time domain, the dynamics of magnetic moments in correlated systems and how to physically interpret the obtained results in terms of their characteristic timescales. Our procedure, exploiting the fluctuation-dissipation theorem, is then applied to clarify the results of INS experiments in several families of iron pnictides and chalcogenides. In particular, the different degrees of discrepancies with respect to the standard *ab initio* calculations is rigorously explained by comparing the timescales of the fluctuating moments to the characteristic timescale of the INS probe. Remarkably, the strong differentiation among the timescales of the materials considered, crucial for a correct understanding of the underlying physics, is almost entirely due to vertex corrections.

While the dynamics of the magnetic moments is particularly intriguing in the Hund's metal materials considered here, the same procedure is directly applicable to all many-electron systems and to fluctuations of different kinds [2]. A precise quantification of the characteristic timescales may provide new keys to connect the findings of equilibrium and out-of-equilibrium spectroscopies, as well as crucial information on the applicability of adiabatic spin dynamics approaches [25].

We thank B. Andersen, L. Boeri, M. Capone, L. de' Medici, P. Hansmann, K. Held, J. Tomczak, and M. Zingl for insightful discussions. We acknowledge support by the Austrian Science Fund (FWF) through Projects No. SFB F41 (C. W., D. S.) and No. I 2794-N35 (A. T.) as well as by the Deutsche Forschungsgemeinschaft (DFG, German Research Foundation) through Grant No. SFB 1170, Projects No. 258499086 and No. EXC 2147, Project No. 390858490 "ct.qmat" (G. S.). Calculations were performed on the Vienna Scientific Cluster (VSC).

[1] A. Hewson, *The Kondo Problem to Heavy Fermions* (Cambridge University Press, 1993).
[2] J. M. Tomczak, arXiv:1904.01346.
[3] M. Imada, A. Fujimori, and Y. Tokura, Rev. Mod. Phys. **70**, 1039 (1998).
[4] A. Georges, G. Kotliar, W. Krauth, and M. J. Rozenberg, Rev. Mod. Phys. **68**, 13 (1996).
[5] P. Hansmann, A. Toschi, G. Sangiovanni, T. Saha-Dasgupta, S. Lupi, M. Maresi, and K. Held, Phys. Status Solidi B **250**, 1251 (2013).
[6] L. de' Medici, J. Mravlje, and A. Georges, Phys. Rev. Lett. **107**, 256401 (2011).
[7] J. Mravlje, M. Aichhorn, and A. Georges, Phys. Rev. Lett. **108**, 197202 (2012).
[8] A. J. Kim, H. O. Jeschke, P. Werner, and R. Valentí, Phys. Rev. Lett. **118**, 086401 (2017).
[9] A. Isidori, M. Berović, L. Fanfarillo, L. de' Medici, M. Fabrizio, and M. Capone, Phys. Rev. Lett. **122**, 186401 (2019).
[10] D. Springer, B. Kim, P. Liu, S. Khmelevskyi, M. Capone, G. Sangiovanni, C. Franchini, and A. Toschi, arXiv:1910.05151.
[11] H. Löhneysen, A. Rosch, M. Vojta, and P. Wölfle, Rev. Mod. Phys. **79**, 1015 (2007).
[12] M. Brando, D. Belitz, F. M. Grosche, and T. R. Kirkpatrick, Rev. Mod. Phys. **88**, 025006 (2016).
[13] J. Kübler, *Theory of Itinerant Electron Magnetism*, International Series of Monogr (Oxford University Press, Oxford, 2000).
[14] A. I. Lichtenstein, M. I. Katsnelson, and G. Kotliar, Phys. Rev. Lett. **87**, 067205 (2001).
[15] A. Hausoel, M. Karolak, E. Şaşıoğlu, A. Lichtenstein, K. Held, A. Katanin, A. Toschi, and G. Sangiovanni, Nat. Commun. **8**, 16062 (2017).
[16] P. A. Lee, N. Nagaosa, and X.-G. Wen, Rev. Mod. Phys. **78**, 17 (2006).
[17] A. Chubukov and P. J. Hirschfeld, Phys. Today **68**, No. 6, 46 (2015).
[18] S. Blundell, *Magnetism in Condensed Matter*, Oxford Master Series in Condensed Matter Physics (Oxford University Press, Oxford, 2001).
[19] R. S. Fishman, J. A. Fernandez-Baca, and T. Ramm, in *Spin-Wave Theory and its Applications to Neutron Scattering and THz Spectroscopy* (Morgan and Claypool Publishers, San Rafael, 2018), Vol. 2053–2571, pp. 2-1 to 2-14.
[20] P. Dai, Rev. Mod. Phys. **87**, 855 (2015).
[21] K. Haule and G. Kotliar, New J. Phys. **11**, 025021 (2009).
[22] R. M. Wilcox, Phys. Rev. **174**, 624 (1968).
[23] M. Sayad and M. Potthoff, New J. Phys. **17**, 113058 (2015).
[24] M. Sayad, R. Rausch, and M. Potthoff, Europhys. Lett. **116**, 17001 (2016).
[25] C. Stahl and M. Potthoff, Phys. Rev. Lett. **119**, 227203 (2017).
[26] See Supplemental Material at http://link.aps.org/supplemental/10.1103/PhysRevLett.125.086402 for further details, which includes Refs. [27–46].
[27] G. Kresse and J. Hafner, Phys. Rev. B **47**, 558 (1993).
[28] G. Kresse and J. Hafner, Phys. Rev. B **49**, 14251 (1994).
[29] A. A. Mostofi, J. R. Yates, G. Pizzi, Y.-S. Lee, I. Souza, D. Vanderbilt, and N. Marzari, Comput. Phys. Commun. **185**, 2309 (2014).

[30] C. Watzenböck, Master's thesis, TU Wien, 2018.
[31] M. T. Czyżyk and G. A. Sawatzky, Phys. Rev. B **49**, 14211 (1994).
[32] S. Li, C. de la Cruz, Q. Huang, Y. Chen, J. W. Lynn, J. Hu, Y.-L. Huang, F.-C. Hsu, K.-W. Yeh, M.-K. Wu, and P. Dai, Phys. Rev. B **79**, 054503 (2009).
[33] X. Wang, Q. Liu, Y. Lv, Z. Deng, K. Zhao, R. Yu, J. Zhu, and C. Jin, Sci. China Phys. Mech. Astron. **53**, 1199 (2010).
[34] V. Grinenko, M. Abdel-Hafiez, S. Aswartham, A. U. B. Wolter-Giraud, C. Hess, M. Kumar, S. Wurmehl, K. Nenkov, G. Fuchs, B. Holzapfel, S. L. Drechsler, and B. Buechner, arXiv:1203.1585.
[35] A. Kowalski, A. Hausoel, M. Wallerberger, P. Gunacker, and G. Sangiovanni, Phys. Rev. B **99**, 155112 (2019).
[36] R. Levy, J. P. F. LeBlanc, and E. Gull, Comput. Phys. Commun. **215**, 149 (2017).
[37] J. Otsuki, M. Ohzeki, H. Shinaoka, and K. Yoshimi, Phys. Rev. E **95**, 061302(R) (2017).
[38] J. Pelliciari, Y. Huang, K. Ishii, C. Zhang, P. Dai, G. F. Chen, L. Xing, X. Wang, C. Jin, H. Ding, P. Werner, and T. Schmitt, Sci. Rep. **7**, 8003 (2017).
[39] K.-W. Yeh, T.-W. Huang, Y.-L. Huang, T.-K. Chen, F.-C. Hsu, P. M. Wu, Y.-C. Lee, Y.-Y. Chu, C.-L. Chen, J.-Y. Luo, D.-C. Yan, and M.-K. Wu, Europhys. Lett. **84**, 37002 (2008).
[40] F. Grønvold, H. Haraldsen, and J. Vihodve, Acta Chem. Scand. **8**, 1927 (1954).
[41] S. Rózsa and H.-U. Schuster, Z. Naturforsch. **36B**, 1668 (1981).
[42] M. Rotter, M. Tegel, D. Johrendt, I. Schellenberg, W. Hermes, and R. Pöttgen, Phys. Rev. B **78**, 020503(R) (2008).
[43] J. H. Tapp, Z. Tang, B. Lv, K. Sasmal, B. Lorenz, P. C. W. Chu, and A. M. Guloy, Phys. Rev. B **78**, 060505(R) (2008).
[44] M. J. Pitcher, D. R. Parker, P. Adamson, S. J. C. Herkelrath, A. T. Boothroyd, R. M. Ibberson, M. Brunelli, and S. J. Clarke, Chem. Commun. (Cambridge) 5918 (2008).
[45] Y. Kamihara, T. Watanabe, M. Hirano, and H. Hosono, J. Am. Chem. Soc. **130**, 3296 (2008).
[46] C. de la Cruz, Q. Huang, J. W. Lynn, J. Li, W. R. II, J. L. Zarestky, H. A. Mook, G. F. Chen, J. L. Luo, N. L. Wang, and P. Dai, Nature (London) **453**, 899 (2008).
[47] P. Werner, E. Gull, M. Troyer, and A. J. Millis, Phys. Rev. Lett. **101**, 166405 (2008).
[48] L. Fanfarillo and E. Bascones, Phys. Rev. B **92**, 075136 (2015).
[49] S. Backes, H. O. Jeschke, and R. Valentí, Phys. Rev. B **92**, 195128 (2015).
[50] L. Boeri, Understanding novel superconductors with *ab initio* calculations, *Handbook of Materials Modeling* (Springer, Cham, 2018).
[51] Y.-T. Tam, D.-X. Yao, and W. Ku, Phys. Rev. Lett. **115**, 117001 (2015).
[52] T. Miyake, K. Nakamura, R. Arita, and M. Imada, J. Phys. Soc. Jpn. **79**, 044705 (2010).
[53] P. Hansmann, R. Arita, A. Toschi, S. Sakai, G. Sangiovanni, and K. Held, Phys. Rev. Lett. **104**, 197002 (2010).
[54] M. Liu, L. W. Harriger, H. Luo, M. Want, R. A. Ewings, T. Guidi, H. Park, K. Haule, G. Kotliar, S. M. Hayden, and P. Dai, Nat. Phys. **8**, 376 (2012).
[55] A. Toschi, R. Arita, P. Hansmann, G. Sangiovanni, and K. Held, Phys. Rev. B **86**, 064411 (2012).
[56] M. Wang, C. Zhang, X. Lu, G. Tan, H. Luo, Y. Song, M. Wang, X. Zhang, E. A. Goremychkin, T. G. Perring, T. A. Maier, Z. Yin, K. Haule, G. Kotliar, and P. Dai, Nat. Commun. **4**, 2874 (2013).
[57] G. Kotliar, S. Y. Savrasov, K. Haule, V. S. Oudovenko, O. Parcollet, and C. A. Marianetti, Rev. Mod. Phys. **78**, 865 (2006).
[58] K. Held, Adv. Phys. **56**, 829 (2007).
[59] M. Wallerberger, A. Hausoel, P. Gunacker, A. Kowalski, N. Parragh, F. Goth, K. Held, and G. Sangiovanni, Comput. Phys. Commun. **235**, 388 (2019).
[60] We compute the dynamical spin-response of the auxiliary impurity model associated to the self-consistent DMFT solution, corresponding to the momentum-averaged one in the limit of high connectivity or dimensions, where DMFT becomes exact [4,61,62].
[61] E. Pavarini, E. Koch, D. Vollhardt, and A. I. Lichtenstein, in *Dmft at 25: Infinite Dimensions: Lecture Notes of the Autumn School on Correlated Electrons* (Forschungszentrum Jülich, Zentralbibliothek, Verlag, 2014), Chap. 4, pp. 91–118.
[62] L. Del Re and A. Toschi (unpublished).
[63] G. Rohringer, A. Valli, and A. Toschi, Phys. Rev. B **86**, 125114 (2012).
[64] D. Springer, P. Chalupa, S. Ciuchi, G. Sangiovanni, and A. Toschi, Phys. Rev. B **101**, 155148 (2020).
[65] t_{INS} is defined—via the energy-time uncertainty principle—as the shortest time interval accessible to an INS process of maximal energy E_{INS} of $\mathcal{O}(100\ \mathrm{meV})$, consistent to most experiments on the materials considered. E_{INS} up to 300 meV was achieved in specific cases [54,56,66].
[66] C. Armstrong, E. Sandqvist, and M. Rheinstadter, Protein Peptide Lett. **18**, 344 (2011).
[67] T. Kroll, S. Bonhommeau, T. Kachel, H. A. Dürr, J. Werner, G. Behr, A. Koitzsch, R. Hübel, S. Leger, R. Schönfelder, A. K. Ariffin, R. Manzke, F. M. F. de Groot, J. Fink, H. Eschrig, B. Büchner, and M. Knupfer, Phys. Rev. B **78**, 220502(R) (2008).
[68] S. Lafuerza, H. Gretarsson, F. Hardy, T. Wolf, C. Meingast, G. Giovannetti, M. Capone, A. S. Sefat, Y.-J. Kim, P. Glatzel, and L. de' Medici, Phys. Rev. B **96**, 045133 (2017).